Surface Fractal Dimensions of Alumina and Aluminum Borate from Nitrogen Isotherms

ARTICLE *in* THE JOURNAL OF PHYSICAL CHEMISTRY B · MAY 1998

Impact Factor: 3.3 · DOI: 10.1021/jp9803485

1 AUTHOR:

Chung-Kung Lee
Vanung University
70 PUBLICATIONS **1,626** CITATIONS

SEE PROFILE

Surface Fractal Dimensions of Alumina and Aluminum Borate from Nitrogen Isotherms

Chung-Kung Lee*

Department of Environmental Engineering, Van-Nung Institute of Technology, Chung-Li, 32054, Taiwan, ROC

Cherng-Shyan Tsay

Department of Chemical Engineering, National Central University, Chung-Li, 32054, Taiwan, ROC

Received: November 26, 1997; In Final Form: March 10, 1998

The effects of calcination temperature on the surface roughness of alumina and aluminum borate samples, prepared by the coprecipitation method and low-water sol−gel processes, were investigated by fractal analysis of their nitrogen adsorption isotherms. The surface fractal dimension *D* was calculated from their nitrogen isotherms using both the fractal isotherm equations derived from the FHH (Frenkel−Halsay−Hill) theory and the recently proposed Neimark equation based on thermodynamics. It was found that for samples calcined from 500 to 1100 °C, the *D* values evaluated using fractal FHH equation were nearly constant (2.5−2.6) despite a large reduction of the BET surface area and pore volume. Only after a 1250 °C calcination, when the α-alumina crystalline phase starts to sinter, was there a slightly larger change of the surface fractal dimension. On the other hand, Neimark's method suggested that thermal effects induce an enormous change on surface roughness of examined samples. The discrepancy of *D* values obtained with the above two methods was discussed.

Introduction

Fractal geometry has been used to describe the structure of porous solid since 1983.[1−3] Significant progress on this subject has been made during the past decade. Both theoretical and experimental studies suggested that the fractal concept is very handy in describing the irregular structure of porous solids. Among the different ways to define a fractal geometry, the term "surface fractal" has been extensively used by Avnir and coworkers to identify the fractal dimension *D* derived from adsorption measurements.[1−3] Usually, the surface fractal dimension *D* is between 2 and 3. A surface with $D = 2$ indicates that it is regular and smooth. A higher *D* value suggests a more wiggle and space-filling surface. At a *D* value close to 3, the surface is extremely irregular. Therefore, the *D* value can be considered as an operative measure of the surface roughness. For instance, it has been found that the *D* value of microporous carbon black changes gradually from 3 to 2 (graphite) upon heating under aerobic conditions.[2]

There are many ways, such as small-angle X-ray and neutron scattering, image analysis, and scanning electron microscopy,[4−7] to determine the surface fractal dimension of a material. However, gas adsorption measurement is one of the techniques more easily available. Within the framework of the gas adsorption method, there are several ways to evaluate the *D* value from the adsorption data.[1,2,8,9] The *D* value can be determined from the monolayer capacities of molecules having different sizes. It can also be calculated from the specific BET surface areas measured on samples having a series of different particle sizes. The third and the most easy way is to fit a single adsorption isotherm to some fractal isotherm equation having *D* as a parameter.

Several fractal isotherm equations have been proposed for such a purpose. Because they are derived on the basis of different physical models concerning multilayer adsorption and capillary condensation, there are still doubts about which one is more suitable and whether a single adsorption isotherm provides enough information to distinguish different morphologies.[10−12] In this study, a series of well-measured nitrogen adsorption isotherms were used to test these different fractal isotherm equations. The isotherms were obtained for both alumina and aluminum borate samples (synthesized with the coprecipitation method and sol−gel process) calcined to different temperatures. These samples thus provide basically the same chemical characteristics but a wide range of pore sizes (from 4 to 50 nm) and surface areas (from 452 to 5 m^2/g). We think it is an ideal platform to critically examine the consistency among these fractal isotherm equations.

Materials and Adsorption Isotherms

The sol−gel process-derived aluminum borate xerogel was prepared from a low-water nonaqueous sol synthesized from aluminum tri(*sec*-butylate) ($Al[OCH(CH_3)C_2H_5]_3$, 97%, Merck, referred to as ATSB in the following), tributyl borate ($B[CH_3(CH_2)_3O]_3$, 99%, Aldrich Chemical Co., referred to as TB in the following), absolute ethanol (C_2H_5OH, >99.8%, Merck), deionized water, and nitric acid (HNO_3, 65%, Merck). The molar proportion of ATSB, TB, H_2O, EtOH, and HNO_3 used is 0.1:0.0111:0.025:10:0.0065, where the water-to-alkoxide ratio is only half that suggested by Yoldas.[13] The details of the synthetic procedure was described elsewhere.[14] The alumina xerogel was synthesized with a similar process except for the absence of TB.[15] On the other hand, the aluminum borate mixed oxide derived by the coprecipitation process was synthesized according to the procedure outlined by Peil et al.[16] The aluminum nitrate ($Al(NO_3)_3 \cdot 9H_2O$, 98.5%, Merck) and boric acid (H_3BO_3, >99.8%, Merck) were mixed with $B/Al = {}^1/_9$, and the pH was controlled to be about 2 with deionized water. An ammonia solution with pH = 11.5 was used as precipitant for

* Corresponding author.

S1089-5647(98)00348-4 CCC: $15.00
Published on Web 05/02/1998

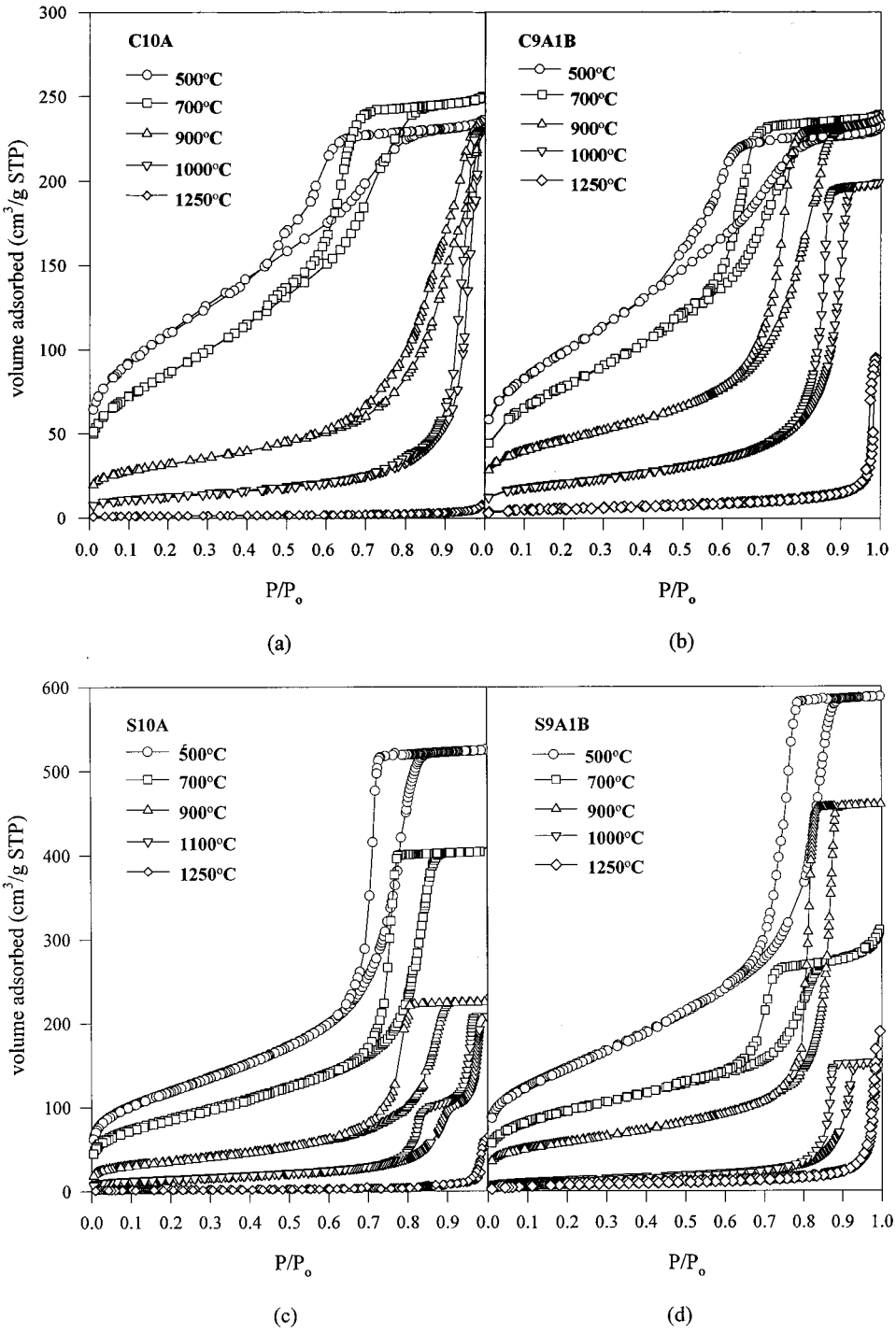

Figure 1. Nitrogen adsorption isotherms of alumina and aluminum borate samples calcined at different temperatures: (a) C10A; (b) C9A1B; (c) S10A; (d) S9A1B. These isotherms suggest that the thermal effect will decrease the BET surface area and pore volume as well as increase the pore size. Moreover, the isotherms also indicate that the pore size distribution of C10A is wider than that of C9A1B, S10A, and S9A1B.

the aluminum boric solution in the coprecipitation process. The two solutions were slowly added to a third container with deionized water to maintain a constant pH of 9. The resulting precipitate was filtered, washed with deionized water (three times), oven-dried at 100 °C for 24 h, and then calcined at a different temperature for 4 h. The alumina was synthesized with a similar process except for the lack of boric acid.

We denote the sol−gel derived alumina and aluminum borate as S10A and S9A1B as well as the coprecipitation method derived counterpart as C10A and C9A1B, respectively.

XRD patterns of the calcined samples were measured by a Siemens D-500 with Cu Kα radiation (30 mA and 40 kV). The nitrogen adsorption isotherm and desorption hysteresis loop was measured at 77 K with a Micromeritics ASAP-2000. All samples were outgassed at 350 °C for 24 h before the adsorption measurement.

Figure 1 shows the nitrogen adsorption−desorption isotherms we have measured on the same alumina and aluminum borate gels calcined at different temperatures. Some key features may be found directly from Figure 1. It can be seen that the monolayer capacity, and thus the BET surface area, decreases with increasing calcination temperature. Also shown are the BET surface areas of samples from the sol−gel process, which are slightly larger than those from the coprecipitation method

TABLE 1: BET Surface Area (m^2/g) of Alumina and Aluminum Borate Obtained from Conventional Analysis of Nitrogen Isotherms

calcination temp (°C)	S10A	S9A1B	C10A	C9A1B
500	430.8	452.5	396.8	358.1
700	311.9	343.8	310.4	286.1
900	128.7	207.3	113.7	166.1
1000		49.2	46.2	75.0
1100	53.5			
1250	8.7	9.3	4.67	20.9

counterparts at low calcination temperature, and the incorporation of boron into the alumina structure with the sol−gel process, which gives a slight increase of the surface area. Table 1 lists the BET surface areas calculated from these isotherms.

All adsorption isotherms except the samples calcined at 1250 °C exhibited obvious capillary condensation at an intermediate relative pressure. The isotherms for the 1250 °C samples showed virtually no uptake until close to saturation pressure, where capillary condensation in the few large voids between α-alumina crystalline grains started. Owing to the increase of condensation pressure with increasing calcination temperature, thermal effects may increase the mean pore size. On the other hand, since uniform pores are identified whenever a steep risor exists in the isotherm (corresponding to the sudden filling of pores that are all of the same size), Figure 1 implies the pore size distribution of S10A, S9A1B, and C9A1B is narrower than that of C10A. Finally, the saturation adsorption capacity in Figure 1 also suggested a decrease of the total pore volume when calcined at higher temperature (except for S9A1B at 900 °C and C10A at 700 °C). Obviously, the densification under heating leads to the simultaneously widening of the pores and the shrinkage of the bulk. There were fewer but generally larger pores after calcination.

For S10A, a two-step isotherm was observed at 1100 °C calcination, leading to a bidisperse pore structure. The appearance of different pore sizes can be understood from the XRD patterns.[14] The gel was completely amorphous after a 700 °C calcination but transformed to γ-alumina at 900 °C. The α-alumina appeared at 1100 °C, and the transformation is completed at 1250 °C. The bidisperse pore structure observed for the 1100 °C sample thus corresponds to the coexistence of two different solid phases. Finally, the alkoxide-derived alumina xerogels (S10A) display a different crystallization route compared with that obtained from the coprecipitation method, as displayed in XRD patterns.[14] The gibbsite and bayerite phases as well as the θ-Al_2O_3 phase are all absent in the transformation to α-alumina.

In our analysis of the nitrogen isotherm, we strive to identify a key parameter that can provide an adequate characterization of surface roughness of alumina and aluminum borate gels for a wide variety of calcination temperatures. A surface fractal is surface irregularities and defects that are characteristically self-similar upon variations of the resolution. According to the data on surface area, the surfaces of examined samples may be approximately divided into smooth (all 1250 °C samples) or rough (500−1100 °C samples). Since the concept of surface irregularity may also be based on a distribution of pore sizes, the rough samples may be further divided into two general categories: roughness due to the presence of uniform pores (S10A, S9A1B, and C9A1B) and roughness due to the presence of a distribution of pore sizes (C10A). In what follows, isotherms recorded on samples are fitted with some fractal isotherm equations to determine whether fractal scaling is present.

Fractal Isotherm Equations

The classical Frenkel−Halsey−Hill (FHH) theory on multilayer adsorption can be extended to fractal surfaces. Two types of fractal isotherm equations have thus been proposed. If the van der Waals attraction between the solid and adsorbed film, which tends to make the gas/film interface replicate the surface roughness, is the dominating factor,[17] one obtains an isotherm equation

$$N/N_m \approx [RT \ln(P_0/P)]^{-(3-D)/3} \quad (1)$$

On the other hand, if the liquid/gas surface tension (capillary force), which tends to move the interface away from the surface to reduce the interface area, is more important,[18] one has

$$N/N_m \approx [RT \ln(P_0/P)]^{-(3-D)} \quad (2)$$

N/N_m represents the surface fractional coverage, and P and P_0 are, respectively, the equilibrium and saturation pressures of the adsorbate. It is known that capillary force usually dominates at higher coverage, and thus, eq 2 should be used at this range. However, eq 2 has also been derived from a fractal extension of the Dubinin−Radushkevich isotherm, which is well-known for the description of micropore filling.[19] In another paper, Yin[20] have presented a derivation for eq 2 from Kelvin's equation with a fractal pore size distribution. Thus, the difference between eqs 1 and 2 can only be verified experimentally.

From the isotherm one can generate a plot of $\ln(N/N_m)$ vs $\ln[\ln(P_0/P)]$. The exponents in eqs 1 and 2 can be obtained from the slope S of this plot. Since $2 \le D < 3$, eq 1 predicts that we should have $-1/3 \le S < 0$, but eq 2 says that $-1 \le S < 0$. It has been argued[17] that when $S = -1/3$, corresponding to a D of 2.67 by eq 2 and $D = 2$ by eq 1, the increase of adsorption due to the capillary condensation is exactly compensated by the reduction of adsorption space due to the fractal characteristic of the surface. It follows that the value of D cannot be unambiguously determined from a single adsorption isotherm when $S \ge -1/3$. Under such conditions, Pfeifer and Cole suggested[18] that the desorption isotherm should also be measured to ensure the presence of capillary condensation within mesopores. Otherwise, the D value should be carefully examined with that obtained by other experimental techniques.

The above fractal isotherm equations have been tested on a number of porous solids, including carbon fibers and carbon blacks,[21−24] silicas,[12,23,25] carbon film,[26] titanium dioxide,[27] cement,[28] clay,[29] and zirconia[30] materials. For most cases, the $\ln(N/N_m)$ vs $\ln[\ln(P_0/P)]$ plot do exhibit a linear portion at higher coverage, but strong curvature is in general observed below or near monolayer coverage. Consequently, the fractal isotherm equation can only be applied within a range of the fractional coverage.[22] Most experimental results show a slope smaller $-1/3$,[31] and the difficulty of determining the dominating mechanism is not present.

For some special cases, the range of linearity is too narrow, and one cannot obtain a D value unambiguously.[12,28] There are also cases (Kr and Ar on aerosols at 77 K) where no linear region can be found at all.[21] It has been proposed that the curvature on the $\ln(N/N_m)$ vs $\ln[\ln(P_0/P)]$ plot may be associated with the coexistence of the surface tension and van der Waals force effects. Therefore, neither eq 1 nor eq 2 completely describes the system. Under such conditions, the best one can say is that the true surface fractal dimension should be between the two limits, or

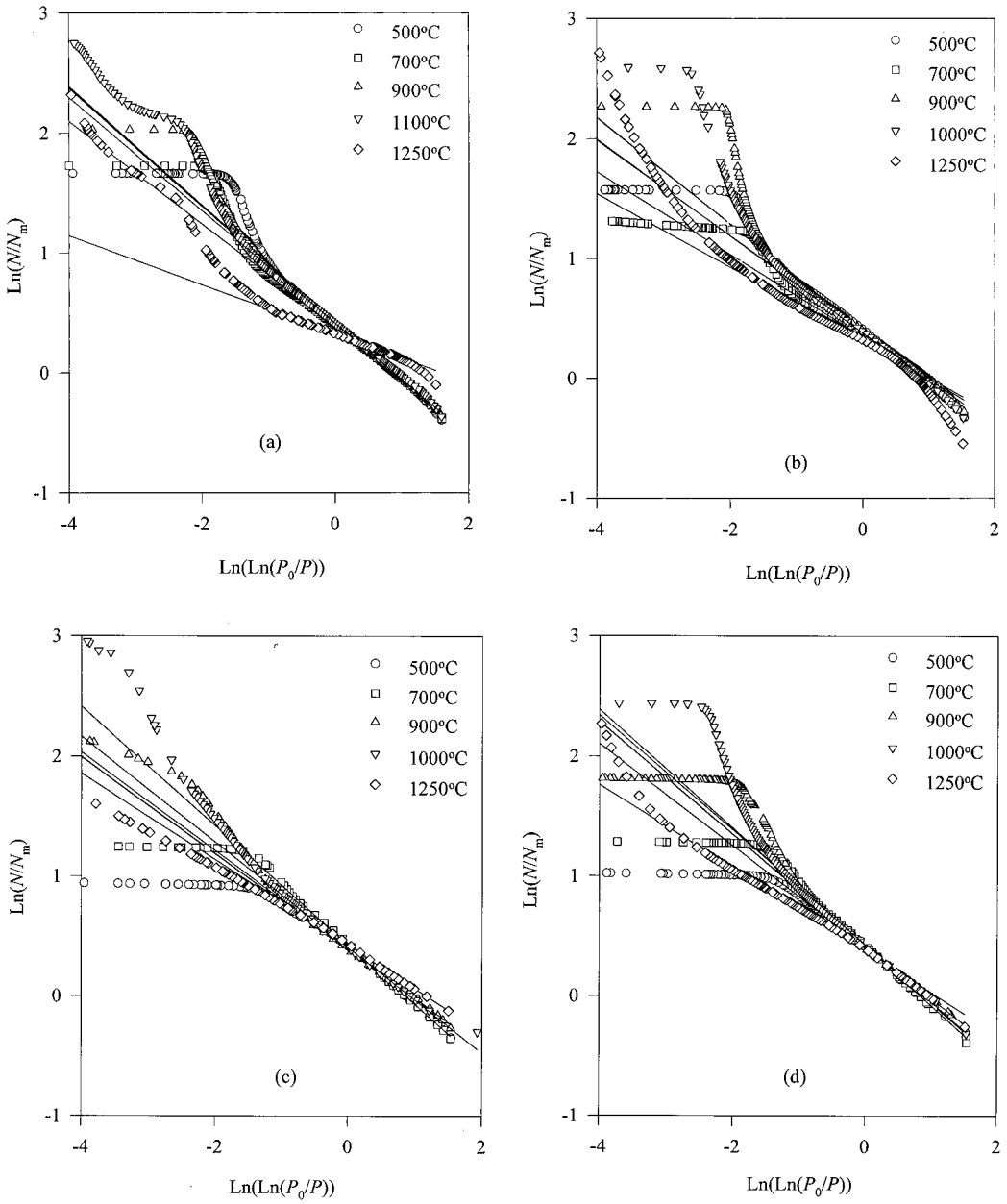

Figure 2. A log−log plot of N/N_m vs ln P/P_0 showing the linear range where fractal behavior is observed: (a) S10A; (b) S9A1B; (c) C10A; (d) C9A1B.

$$3(1 + S) \leq D \leq 3 + S \tag{3}$$

Ismail and Pfeifer[21] have suggested that the effect of surface tension on D is negligible if $S \geq -1/3$ and is important otherwise. A more detailed theory[18] predicts that the switching from the capillary force dominated regime to the van der Waals force dominated regime occurs at

$$N/N_m = \left[\frac{\beta\rho}{(D-2)\gamma t^2}\right]^{(3-D)/2} \tag{4}$$

where β is the van der Waals constant for the gas/solid interaction, ρ is the density of liquid nitrogen film, γ is the liquid/gas surface tension, and t is the thickness of one adsorbed layer. Accordingly, the onset of capillary condensation occurs at higher N/N_m values for a surface with lower surface fractal dimension.

In addition to the fractal FHH equations discussed above, Neimark[32,33] has recently proposed a so-called thermodynamic fractal isotherm equation. The basis for this equation is a very simple relationship between the area of the gas/liquid interface A and the mean radius of the curvature of this interface r

$$\ln A = \text{const} - (D-2)\ln r \tag{5}$$

In this equation, the area of the gas/liquid interface can be calculated according to the Kiselev equation:

$$A = (RT/\gamma)\int_{N(P/P_0)}^{N_{max}} \ln(P_0/P)\, dN \tag{6}$$

where N_{max} denotes the amount adsorbed when P/P_0 approaches unity. At the same time, the Kelvin equation is used to convert the equilibrium pressure P to the mean radius of the curvature r. Applications of Neimark's equation to evaluate D have been demonstrated in refs 34 and 35.

Neimark's equation is based on the free energy of the liquid/gas interface and thus assumes the same adsorption mechanism, namely, capillary condensation, as does eq 2. Indeed, recently,

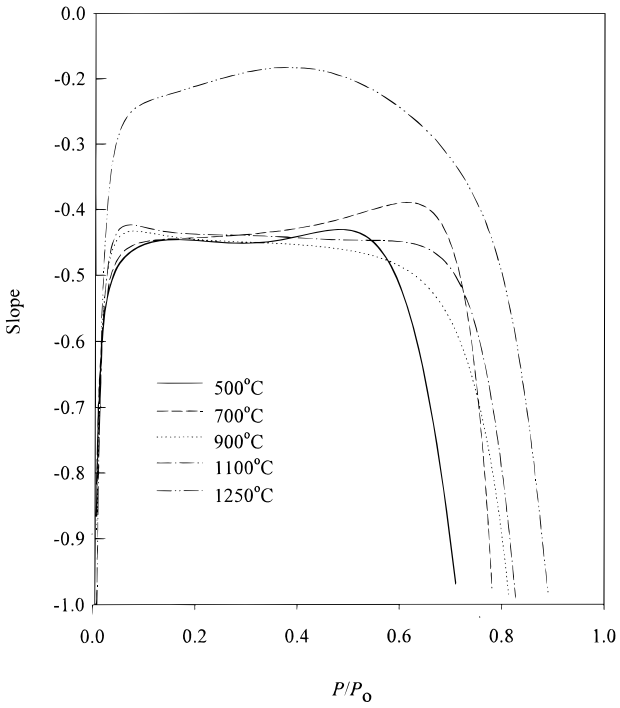

Figure 3. Variation of local slope in Figure 2a as a function of P/P_0. Surface fractal dimension can be calculated from the average slope in the range where there are only small variations.

it has been shown theoretically by Jaroniec[36] and experimentally by Sahouli et al.[37] that the same results were obtained in the capillary condensation regime by the Neimark's equation and by the fractal FHH equation with a $-(3 - D)$ exponent.

Surface Fractal Dimension Calculation

The N/N_m vs ln P_0/P plots of all isotherms are given in Figure 2 in double-logarithmic scales. Because there were enough data to trace the entire isotherm, one can easily fit the curve and calculate its local slope. Therefore, instead of arbitrarily choosing a range to find the average slope, the variation of the local slope can be calculated. One example was given in Figure 3 for S10A. From this figure, one can be sure that there is a large range of relative pressures where the slope is nearly a constant. These constant slopes are nearly the same for different calcination temperatures except for the 1250 °C one. However, the range of relative pressures where linearity is observed is different for each calcination temperature. At small and large relative pressures, the slope dropped very sharply. The deviation from linearity at low relative pressures can be understood by the fact that below monolayer coverage the isotherm is governed by a combination of attractive and repulsive gas/solid interactions and thus no longer probes the surface geometry effectively.[21]

The surface fractal dimension can now be calculated from the constant slopes with either eq 1 or eq 2. The results were collected in Table 2 for all alumina and aluminum borate samples. Also given were the range of P/P_0 and the length scale where fractal characteristics, i.e., a linear behavior in double-logarithmic scales, was observed. These length scales were computed from the number of adsorbed layers, $n \equiv (N/N_m)^{1/(3-D)}$, and the N_2 layer thickness of 0.35 nm.[18] Note that when fractal behavior is observed in the capillary-force-controlled regime, the coverage is always above monolayer capacity. Thus, the calculated length scale is always larger than the N_2 molecular size.

According to Table 2, the constant slopes in the linear range are all smaller than $-1/3$ except for the 1250 °C samples. This suggests that eq 1 is not applicable for these isotherms, and eq 2 should be used. For the case of the 1250 °C sample the slope is larger than $-1/3$, and its desorption isotherm suggests negligible capillary condensation in the mesopore range. Accordingly, we should use eq 1 to evaluate D. The key feature in Table 2 is that the D values obtained with the fractal FHH equation are nearly constant (2.5−2.6) except for the 1250 °C one, indicating that the surface fractal dimensions of alumina and aluminum borate were rather stable upon calcination until the appearance of the α-alumina phase. Another interesting feature is that the length scale at 1250 °C is smaller than that of another calcination temperature for each sample.

Let us now look at the results calculated by Neimark's equation. In Figure 4 we have plotted the interface area verses the radius of curvature in double-logarithmic scales for all isotherms. The variation of local slope with P/P_0 is given in Figure 5 for S10A. Again, there is a range where the slopes are effectively constants. The D values correspond to the constant slopes in the linear portion, and the range of scale exhibiting fractal behavior can again be calculated as given in

TABLE 2: Surface Fractal Dimensions of Alumina and Aluminum Borate Obtained Using Fractal FHH Isotherm Equations

sample	calcination temp (°C)	slope	D from eq 1	D from eq 2	applicable range of P/P_0	applicable range of N/N_m	length scale (nm)
S10A	500	−0.45	(1.66)	2.55	0.09−0.56	1.00−1.90	0.35−1.47
	700	−0.44	(1.69)	2.56	0.09−0.56	1.00−1.84	0.35−1.41
	900	−0.45	(1.64)	2.55	0.09−0.63	1.01−2.12	0.35−1.84
	1100	−0.44	(1.67)	2.56	0.08−0.70	1.00−2.42	0.35−2.58
	1250	−0.20	2.38	(2.80)	0.07−0.55	1.12−1.53	1.07−1.28
S9A1B	500	−0.44	(1.67)	2.56	0.04−0.82	1.00−3.87	0.35−7.40
	700	−0.37	(1.90)	2.63	0.08−0.52	1.00−1.65	0.35−1.37
	900	−0.40	(1.80)	2.60	0.07−0.66	1.00−2.10	0.35−2.24
	1000	−0.40	(1.78)	2.60	0.09−0.61	1.00−1.93	0.35−1.77
	1250	−0.31	2.07	(2.70)	0.20−0.85	4.23−9.00	1.72−2.29
C10A	500	−0.40	(1.79)	2.60	0.09−0.70	1.00−2.18	0.35−2.40
	700	−0.50	(1.51)	2.50	0.09−0.70	1.00−2.59	0.35−2.37
	900	−0.41	(1.77)	2.59	0.10−0.70	1.00−2.31	0.35−2.69
	1000	−0.44	(1.68)	2.56	0.08−0.70	1.00−2.37	0.35−2.48
	1250	−0.31	2.05	(2.68)	0.30−0.90	1.43−3.16	0.51−1.17
C9A1B	500	−0.47	(1.59)	2.53	0.09−0.61	1.00−2.06	0.35−1.62
	700	−0.50	(1.51)	2.51	0.11−0.66	1.00−2.38	0.35−2.02
	900	−0.43	(1.72)	2.57	0.07−0.64	1.00−2.15	0.35−2.11
	1000	−0.48	(1.56)	2.52	0.07−0.80	1.00−3.40	0.35−4.50
	1250	−0.32	2.02	(2.67)	0.33−0.92	1.41−3.46	0.50−1.25

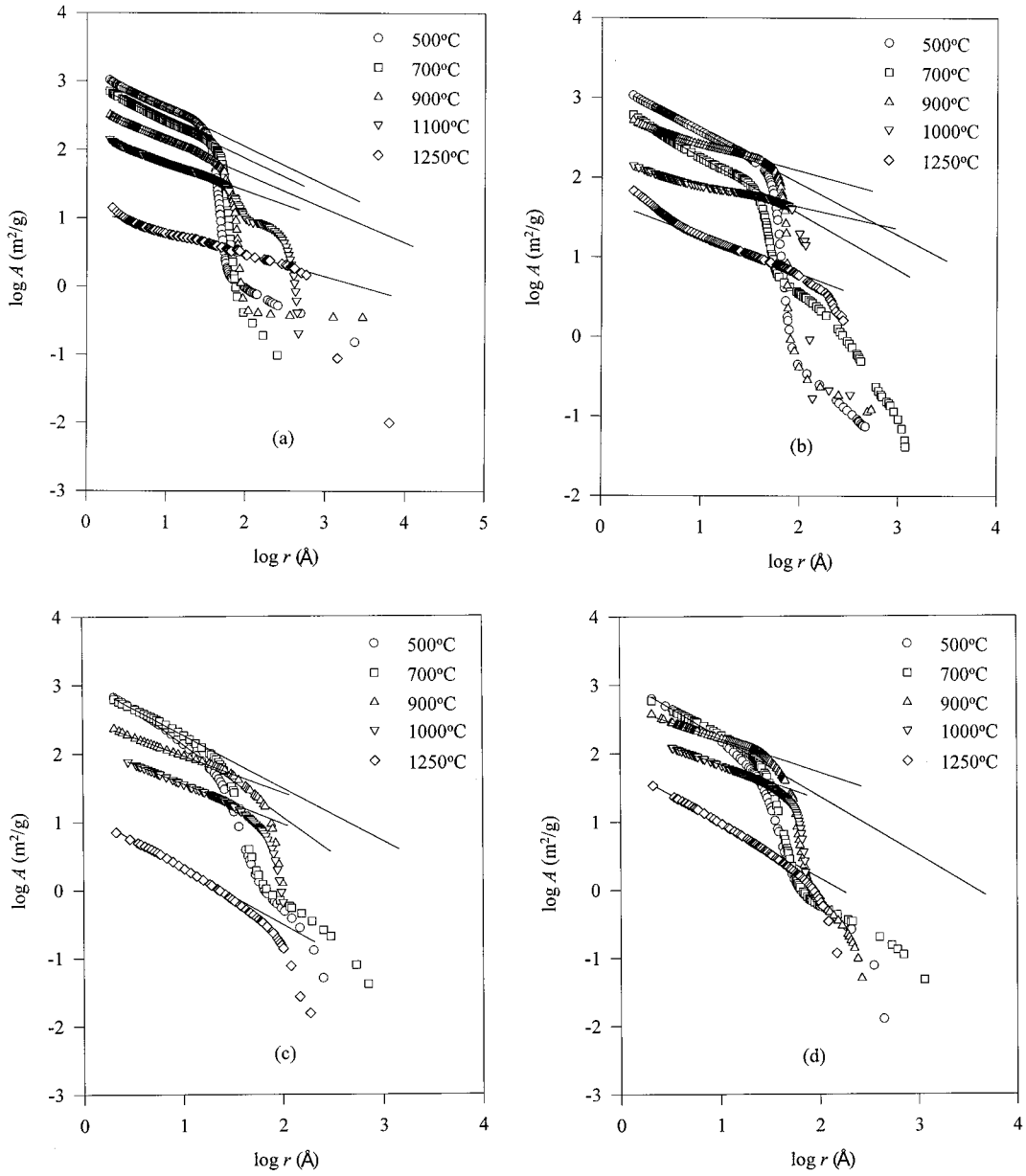

Figure 4. Plots drawn with the standard coordinates of the thermodynamic method, log A vs log r, with the straight lines corresponding to the linear regression in the scale range of possible fractality: (a) S10A; (b) S9A1B; (c) C10A; (d) C9A1B.

Table 3 for all samples. As listed in Table 3, D values exhibit an obvious change with increasing calcination temperature, implying that the heating treatment greatly affects the surface irregularity.

By comparison of Tables 2 and 3, it was found that the D values obtained from Neimark's equation disagree with those calculated from the fractal FHH equations except for S10A at all temperatures and both C10A and C9A1B at 900−1000 °C.

Sahouli et al.[37] have also observed the disagreement between D values obtained by Neimark's equation and that by fractal FHH equations. They attribute the differences to the large amount of micropores present in their carbon black samples. Because the fractal FHH equations are sensitive to the microporous structures and if the adsorption is controlled by both van der Waals attraction and capillary condensation, the effect of microporosity cannot be neglected. However, our samples contain virtually no micropores, so the effect they claimed should not exist. Therefore, more discussions are needed for the discrepancy between the two methods.

The fractal FHH equation for the capillary condensation regime and Neimark's model are derived by using the Kelvin equation in a different fractal definition. The FHH equation uses the film volume or the pore size distribution to define fractal, while Neimark introduces the fractal definition of surface area of the adsorbed film. Accordingly, the FHH type equation might be sensitive to the pore size distribution. For porous materials, any rough surface might be considered as a smooth surface that has been crumpled. Alternatively, the same rough surface may be considered to consist of a distribution of pores of varying radii. Therefore, pore size distribution can contribute significantly to the surface fractal dimension. For the C10A sample, a wide pore size distribution was found at different temperatures. This most probably explains the disagreement between D values obtained with the two methods. On the other hand, the pore network of another examined sample is constituted of channels with a relatively narrow size distribution and the fractality thus reflects the roughness of the primary particle but not the geometry of the pore network. In this case, the

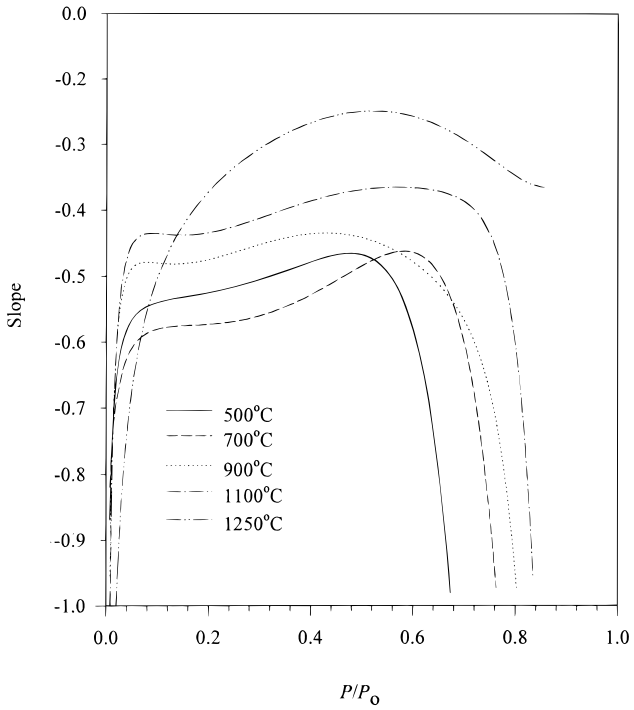

Figure 5. Variation of local slope in Figure 4a as a function of P/P_0. Surface fractal dimension can be calculated from the average slope in the range where there are only small variations.

TABLE 3: Surface Fractal Dimensions of Alumina and Aluminum Borate Obtained Using the Neimark's Equation

sample	calcination temp (°C)	D	applicable range of P/P_0	applicable range of r (nm)
S10A	500	2.53	0.09−0.46	0.40−1.24
	700	2.55	0.09−0.60	0.40−1.91
	900	2.47	0.09−0.61	0.40−1.95
	1100	2.41	0.09−0.65	0.40−2.21
	1250	(2.32)	0.20−0.82	0.59−4.95
S9A1B	500	2.65	0.09−0.60	0.40−1.87
	700	2.70	0.09−0.60	0.40−1.87
	900	2.35	0.09−0.62	0.40−2.03
	1000	2.27	0.09−0.64	0.40−2.18
	1250	(2.47)	0.30−0.82	0.79−4.91
C10A	500	2.99	0.09−0.60	0.40−1.88
	700	2.78	0.09−0.54	0.40−1.57
	900	2.54	0.09−0.55	0.40−1.59
	1000	2.59	0.09−0.72	0.40−2.97
	1250	(2.86)	0.09−0.73	0.40−2.99
C9A1B	500	2.86	0.09−0.35	0.40−0.91
	700	2.75	0.09−0.40	0.40−1.03
	900	2.46	0.09−0.69	0.40−2.55
	1000	2.54	0.09−0.69	0.40−2.55
	1250	(2.86)	0.09−0.69	0.40−2.56

mean radius of pore channels is the upper limit of possible fractality. Since XRD patterns show the coexistence of some distinct solid phases before the transformation to α-alumina is completed,[14] the discrepancy between the two methods in the cases of S10A, S9A1B, and C9A1B samples might be explained by the existence of mixing solid phases during the heating treatment process. More generally, discrepancies between D values obtained from eq 2 and those obtained from eq 5 are expected whenever the surface possesses nonfractal features at large length scales. The reason is that the area A in Neimark's equation is calculated from integration of the coverage in all large pores (eq 6) so that A includes contributions from nonfractal features if such are present. The limited range of length scales in which the data obey the FHH isotherms and Neimark's equation, typically less than 10 nm (last column in Tables 2 and 3), indicates that the investigated surfaces do contain a significant amount of nonfractal structure at large scales. The limited range also suggests that the fractal interpretation should perhaps be regarded as provisional, awaiting additional tests.

It is worth noting that for all 1250 °C samples, the surface fractal dimension characterizes the roughness of the external surface of the particles in a relatively wide scale range, since the crystallization of α-alumina, which possess low BET surface area and low porosity, is completed after this temperature. As mentioned above, the application of Neimark's equation is questionable in this case and the fractal FHH equation with exponent $-(3 - D)/3$ was suggested for evaluating the surface fractal dimension.

For alumina and aluminum borate materials generated by the sol−gel process, the gelation can take place either by chemical branching or by physical aggregation of primary particles. A solid material is then obtained by drying and sintering. On the other hand, the coprecipitation method is mainly aggregates of small primary colloidal particles. In accordance with Table 1 it is clear that materials made by the sol−gel process and the coprecipitation method are chemically identical, but their surface properties are drastically different. This fact is a result of different kinetic growth processes of the primary particles. These kinetic growth processes can produce mass fractals and can also give surface fractals.

The surface roughness is well characterized by the D values. If the D values are constant at different calcination temperatures, i.e., the initial roughness of the primary particles is maintained at high heating temperatures, the decrease in the BET surface area must only be due to collapse of different pore sizes. This result is concluded from the analysis of fractal FHH equation. In contrast, if the D values decrease with increasing temperatures, as shown in the analysis of our samples with Neimark's method, both the smoothing of surface roughness and the disappearance of different pore sizes can spontaneously contribute to the decrease of surface area. It was noteworthy that this result was also observed by Rubio et al.[30] in the analysis of their zirconia materials.

The implication of the above fractal analyses is that the surfaces of alumina and aluminum borate are indeed irregular and may be described by a fractal geometry in a limited range of length scale. However, thermal effects on D values is difficult to identify only from BET surface area data, since the decrease of surface area may be due to the shrinkage of the pores and the smoothing of their surface roughness, and how to quantitatively distinguish the contributions from these two factors is difficult. Thus, other experimental techniques are needed to further check the heating effect on the surface roughness.

Conclusions

Different fractal isotherm equations have been tested with well-measured nitrogen isotherms on alumina and aluminum borate samples. For different isotherms, a choice must be made between the two fractal FHH equations to assess the surface fractal dimension. When an appropriate fractal FHH equation was used, the values of D determined are nearly the same for all examined samples except at 1250 °C, implying that surface roughness is unaffected with heating treatment before the sintering between α-alumina crystals occurred. On the other hand, the D values evaluated with the Neimark's method indicated that thermal effects might induce a large reduction in the surface roughness. The disagreement between the two

methods is ascribed to the pore size distribution effect (for C10A) or the coexistence of different solid phases during the calcination process (for S10A, S9A1B, and C9A1B). Because the *D* values evaluated with different fractal isotherms are not consistent, the results must be interpreted with caution and other independent experiments are needed to provide more confidence.

Acknowledgment. The work was supported by Grant NSC86-2214-E-238-001 of the National Science Council (Taiwan, ROC).

References and Notes

(1) Pfeifer, P.; Avnir, D. *J. Chem. Phys.* **1983**, *79*, 3558.
(2) Avnir, D.; Farin, D.; Pfeifer, P. *J. Chem. Phys.* **1983**, *79*, 3566.
(3) Avnir, D.; Farin, D.; Pfeifer, P. *Nature* (*London*) **1984**, *308*, 261.
(4) Avnir, D., Ed. *The Fractal Approach to Heterogeneous Chemistry*: *Surfaces, Colloids, Polymers*; John Wiley: Chichester, 1989.
(5) Bunde, A., Havlin, S., Eds. *Fractals and Disordered Systems*; Springer: Berlin, 1991.
(6) Avnir, D.; Farin, D. *New J. Chem.* **1990**, *14*, 197.
(7) Avnir, D.; Farin, D.; Pfeifer, P. *New J. Chem.* **1992**, *16*, 439.
(8) Lee, C. K.; Chiang, A. S. T.; Tsay, C. S. In *Key Engineering Materials*; Liu, D. M., Ed.; Trans Tech Publications: Switzerland, 1996; Vol. 115, pp 21−44.
(9) Lee, C. K.; Lee, S. L. *Heterog. Chem. Rev.* **1996**, *3*, 269.
(10) Drake, J. M.; Levitz, P.; Klafter, J. *New J. Chem.* **1990**, *14*, 77.
(11) Drake, J. M.; Levitz, P.; Klafter, J. *Isr. J. Chem.* **1991**, *31*, 135.
(12) Drake, J. M.; Yacullo, L. N.; Levitz, P.; Klafter, J. *J. Phys. Chem.* **1994**, *98*, 380.
(13) Yoldas, B. E. In *Ultrastructure Processing Advanced Ceramic*; Mackenzie, J. D., Ulrich, D. R., Eds.; Wiley & Sons: New York, 1988; p 333.
(14) Lee, C. K.; Tsay, C. S. *J. Chem. Soc., Faraday Trans.*, in press.
(15) Tsay, C. S.; Lee, C. K.; Chiang, A. S. T. *Chem. Phys. Lett.* **1997**, *278*, 83.
(16) Peil, K. P.; Galya, L. G.; Marcelin, G. *J. Catal.* **1989**, *115*, 441.
(17) Pfeifer, P.; Wu, J.; Cole, M. W.; Krim, J. *Phys. Rev. Lett.* **1989**, *62*, 1997.
(18) Pfeifer, P.; Cole, M. W. *New J. Chem.* **1990**, *14*, 221.
(19) Avnir, D.; Jaroniec, M. *Langmuir* **1989**, *5*, 1431.
(20) Yin, Y. *Langmuir* **1991**, *7*, 216.
(21) Ismail, I. M. K.; Pfeifer, P. *Langmuir* **1994**, *10*, 1532.
(22) Kaneko, K.; Sato, M.; Suzuki, T.; Fujiwara, Y.; Nishikawa, K.; Jaroniec, M. *J. Chem. Soc., Faraday Trans.* **1991**, *87*, 179.
(23) Ehrburger-Dolle, F.; Holz, M.; Lahaye, J. *Pure Appl. Chem.* **1993**, *65*, 2223.
(24) Darmstadt, H.; Roy, C.; Kaliaguine, S.; Sahouli, B.; Blacher, S.; Pirard, R.; Brouers, F. *Rubber Chem. Technol.* **1995**, *68*, 330.
(25) Lefebvre, Y.; Lacelle, S.; Jolicoeur, C. *J. Mater. Res.* **1992**, *7*, 1888.
(26) Wang, C. L.; Krim, J.; Toney, M. F. *J. Vac. Sci. Technol. A* **1989**, *7*, 2481.
(27) Wu, M. K. *Aerosol Sci. Technol.* **1996**, *25*, 392.
(28) Niklasson, G. A. *Cem. Concr. Res.* **1993**, *23*, 1153.
(29) Celis, R.; Cornejo, J.; Hermosin, M. C. *Clay Miner.* **1996**, *31*, 355.
(30) Rubio, F.; Rubio, J.; Oteo, J. L. *J. Mater. Sci. Lett.* **1997**, *16*, 49.
(31) Gregg, S. J., Sing, K. S. W., Eds. *Adsorption, Surface Area and Porosity*, 2nd ed.; Academic Press: New York, 1982; p 90.
(32) Neimark, A. V. *JETP Lett.* **1990**, *51*, 607.
(33) Neimark, A. V. *Adsorpt. Sci. Technol.* **1991**, *7*, 210.
(34) Neimark, A. V.; Unger, K. K. *J. Colloid Interface Sci.* **1993**, *150*, 412.
(35) Neimark, A. V.; Hanson, M.; Unger, K. K. *J. Phys. Chem.* **1993**, *97*, 6011.
(36) Jaroniec, M. *Langmuir* **1995**, *11*, 2316.
(37) Sahouli, B.; Blacher, S.; Brouers, F. *Langmuir* **1996**, *12*, 2872.